Shifted nondiffractive Bessel beams

Alexey A. Kovalev, Victor V. Kotlyar, and Alexey P. Porfirev
Laser Measurements Laboratory, Image Processing Systems Institute, Russian Academy of Sciences, 151 Molodogvardejskaya street, Samara, Russia, 443001
and Technical Cybernetics sub-department, S.P. Korolyov Samara State Aerospace University (National Research University), 34 Moskovskoye shosse, Samara, Russia, 443086
(Received 3 March 2015; published 21 May 2015; corrected 22 June 2016)

Nondiffractive Bessel beams are well known to have infinite energy and infinite orbital angular momentum (OAM). However, when normalized to unity of energy, their OAM is finite. In this work, we derive an analytical relationship for calculating the normalized OAM of the superposition of off-axis Bessel beams characterized by the same topological charge. We show that if the constituent beams of the superposition have real-valued weight coefficients, the total OAM of the superposition of the Bessel beams equals that of an individual nonshifted Bessel beam. This property enables generating nondiffractive beams with different intensity distributions but identical OAM. The superposition of a set of identical Bessel beams centered on an arbitrary-radius circle is shown to be equivalent to an individual constituent Bessel beam put in the circle center. As a result of a complex shift of the Bessel beam, the transverse intensity distribution and OAM of the beam are also shown to change. We show that, in the superposition of two or more complex-shifted Bessel beams, the OAM may remain unchanged, while the intensity distribution is changed. Numerical simulation is in good agreement with theory.

DOI: 10.1103/PhysRevA.91.053840 PACS number(s): 42.50.Tx, 42.60.Jf, 42.25.Fx

I. INTRODUCTION

Bessel beams, discovered in 1987 [1,2], possess a variety of remarkable properties. They travel without diffraction over a certain distance in free space [1] and generate optical tubes or cavities on the optical axis [3,4], also featuring a property of self-healing following a distortion caused by a minor obstacle [5,6].

Bessel beams have an orbital angular momentum (OAM) [7,8]. The superposition of Bessel beams can be axially periodic (analog of the Talbot effect) [9,10] or experience rotation about the optical axis upon propagation [11,12].

Bessel beams can be generated using digital holograms [3,4,13], a conical refractive axicon [14,15], a diffractive vortex axicon [16], diffractive optical elements [11,12], and spatial light modulators [17]. It is interesting that astigmatic Bessel beams can be generated by simply tilting the diffractive element or illuminating the diffractive vortex axicon by a tilted beam [18].

Bessel beams have found a variety of applications. One of the uses is for micromanipulation intended for simultaneously trapping several microparticles on the optical axis [19,20] or rotating individual, or a number of, microparticles about the optical axis [21]. Using Bessel beams, it is possible to trap and accelerate individual cooled atoms [22,23]. Recently proposed Hankel-Bessel beams [24] may find use in atmospheric probing because they are immune to atmospheric turbulence [25]. Theoretical analysis of vector Bessel beams was for the first time conducted in Refs. [26,27] and analytical relations for the OAM density were derived in Refs. [7,8,28]. It should be noted that because the total energy of a Bessel beam is infinite, total OAM is also infinite. Because of this, prior to the present work, no study of OAM of the entire Bessel beams has previously been conducted. As well as defining eigenfunctions for circular billiards, Bessel modes also represent resonant geometric modes that possess OAM [29].

More recently, nonparaxial asymmetric Bessel modes [30] and paraxial asymmetric Bessel-Gaussian beams [31] have been proposed. These laser beams have been shown to produce the transverse intensity pattern in the form of a semicrescent. In Ref. [32], the asymmetric Bessel modes were studied experimentally using a digital micromirror array. By analogy with Ref. [30], asymmetric Chebyshev-Bessel beams have also been proposed [33].

Previously, study of the superposition of axial Bessel beams has only been reported [10–12,19,28]. The study of the superposition of off-axis laser beams discussed in Ref. [29] did not involve Bessel beams.

In this work, we analyze the superposition of off-axis Bessel beams of the same order and topological charge. A general analytical expression for the OAM of the superposition under study has been derived. We show that if the constituent beams of the superposition have real-valued weight coefficients, the total OAM of the superposition of the Bessel beams equals that of an individual nonshifted Bessel beam. This property enables generating nondiffractive beams with different intensity distributions but identical OAM. The superposition of a set of identical Bessel beams centered on an arbitrary-radius circle is shown to be equivalent to an individual constituent Bessel beam put in the circle center. As a result of a complex shift of the Bessel beam, the transverse intensity pattern and OAM of the beam are also shown to change. We show that in the superposition of two or more complex-shifted Bessel beams, the OAM may remain unchanged, while the intensity distribution is changed. Numerical simulation is in good agreement with theory.

II. FOURIER SPECTRUM OF A SHIFTED BESSEL BEAM

The complex amplitude of a nonparaxial stationary light field that satisfies the Helmholtz equation has been known to be expressed as the angular spectrum of plane

waves [34]:

$$E(x,y,z) = \iint_{\mathbb{R}^2} A(\xi,\eta)\exp[ik(\xi x + \eta y + ikz\sqrt{1-\xi^2-\eta^2})]\,d\xi\,d\eta, \quad (1)$$

where k is the wave number of monochromatic light and $A(\xi,\eta)$ is the complex amplitude of the angular spectrum of plane waves. In polar coordinates (r,ϕ), Eq. (1) takes the form:

$$E(r,\phi,z) = \iint_{\mathbb{R}^2} A(\rho,\theta)\exp[ikr\rho\cos(\theta-\phi) + ikz\sqrt{1-\rho^2})]\rho\,d\rho\,d\theta, \quad (2)$$

where (ρ,θ) are the polar coordinates in the Fourier plane. If the beam is shifted from the axis by a Cartesian vector (x_0,y_0), the amplitude of the angular spectrum of plane waves is given by

$$A'(\rho,\theta) = A(\rho,\theta)\exp[-ik\rho(x_0\cos\theta + y_0\sin\theta)], \quad (3)$$

where $A(\rho,\theta)$ is the amplitude of the angular spectrum of plane waves for the original nonshifted beam. Note that the shift coordinates (x_0,y_0) may take complex values.

The angular spectrum of a nonshifted n-order Bessel beam has been known [30] to be given by

$$A_n(\rho,\theta) = \frac{(-i)^n}{\alpha\lambda}\exp(in\theta)\delta\left(\rho - \frac{\alpha}{k}\right), \quad (4)$$

where $\delta(x)$ is the Dirac δ function and α is the scale factor of the nonshifted Bessel mode

$$E_n(r,\phi,z) = \exp(in\phi + iz\sqrt{k^2-\alpha^2})J_n(\alpha r), \quad (5)$$

where $J_n(x)$ is the n-order Bessel function of the first kind. In view of Eq. (3), the amplitude of the angular spectrum of the shifted n-order Bessel beam is

$$A'_n(\rho,\theta) = \frac{(-i)^n}{\alpha\lambda}\exp(in\theta)\delta\left(\rho - \frac{\alpha}{k}\right) \times \exp[-ik\rho(x_0\cos\theta + y_0\sin\theta)]. \quad (6)$$

III. RELATION BETWEEN THE AMPLITUDES OF SPECTRA OF SHIFTED AND NONSHIFTED BESSEL BEAMS

We shall find coefficients A_{mn} of a series that describes the expansion of the amplitude of the spectrum of a shifted n-order Bessel beam (6) in terms of the amplitudes of the spectrum of the nonshifted different-order Bessel beams:

$$A'_n(\rho,\theta) = \delta\left(\rho - \frac{\alpha}{k}\right)\sum_{p=-\infty}^{\infty} A_{pn}\frac{(-i)^p}{\alpha\lambda}\exp(ip\theta). \quad (7)$$

Multiplying both sides of Eq. (7) by $[\alpha\lambda/\delta(\rho-\alpha/k)]\exp(-im\theta)$ and integrating over θ from 0 to 2π we obtain:

$$\int_0^{2\pi}\exp[i(n-m)\theta - i\alpha(x_0\cos\theta + y_0\sin\theta)]d\theta = i^n\sum_{p=-\infty}^{\infty} A_{pn}(-i)^p 2\pi\delta_{pm}. \quad (8)$$

In the left-hand side of Eq. (8), we have

$$\int_0^{2\pi}\exp(in\theta + ia_0\cos\theta + ib_0\sin\theta)d\theta = 2\pi\left(\frac{ia_0-b_0}{\sqrt{a_0^2+b_0^2}}\right)^n J_n\left(\sqrt{a_0^2+b_0^2}\right), \quad (9)$$

where a_0 and b_0 are some constants (not necessarily real).

In view of Eq. (9), the coefficients in the right-hand side of Eq. (8) are

$$A_{mn} = \left(\frac{x_0+iy_0}{\sqrt{x_0^2+y_0^2}}\right)^{n-m} J_{m-n}\left(\alpha\sqrt{x_0^2+y_0^2}\right). \quad (10)$$

In particular, if the same-value shift is real on one coordinate and imaginary on the other $(x_0 = c/\alpha, y_0 = ic/\alpha)$, the coefficients in Eq. (10) are simplified to

$$A_{mn} = \begin{cases} \frac{c^{m-n}}{(m-n)!} & \text{if} \quad m \geqslant n, \\ \delta_{nm} & \text{if} \quad m \leqslant n. \end{cases} \quad (11)$$

In this particular case, the amplitude of the angular spectrum of plane waves for the shifted Bessel beam can be represented by a linear combination of the spectrum of the different-order Bessel modes:

$$A'_n(\rho,\theta) = \delta\left(\rho - \frac{\alpha}{k}\right) \times \sum_{p=0}^{\infty}\frac{c^p}{p!}\frac{(-i)^{n+p}}{\alpha\lambda}\exp[i(n+p)\theta], \quad (12)$$

with the parameter c defining the degree of asymmetry of the shifted n-order Bessel mode. The angular spectrum of the shifted Bessel mode in Eq. (12) is seen to be identical to that of an asymmetric Bessel mode [30].

Rearranging Eq. (1) with use of Eqs. (6) and (9), we obtain the relationship for the amplitude of the shifted Bessel beam:

$$E'_n(x,y,z) = \exp(iz\sqrt{k^2-\alpha^2}) \times \left[\frac{(x-x_0)+i(y-y_0)}{\sqrt{(x-x_0)^2+(y-y_0)^2}}\right]^n \times J_n(\alpha\sqrt{(x-x_0)^2+(y-y_0)^2}). \quad (13)$$

IV. ORBITAL ANGULAR MOMENTUM OF A SHIFTED BESSEL BEAM

Projection of OAM on the optical axis z and total power of the laser beam can be found from the relations [30]:

$$iJ_z = \iint_{\mathbb{R}^2} E^*\frac{\partial E}{\partial\phi}rdrd\phi = \left(\frac{2\pi}{k}\right)^2\iint_{\mathbb{R}^2} A^*\frac{\partial A}{\partial\theta}\rho d\rho d\theta, \quad (14)$$

$$W = \iint_{\mathbb{R}^2} E^*Erdrd\phi = \left(\frac{2\pi}{k}\right)^2\iint_{\mathbb{R}^2} A^*A\rho d\rho d\rho d\theta, \quad (15)$$

When calculating Eqs. (14) and (15) for the shifted Bessel beam, we shall utilize Eq. (6). Then the projection of OAM

onto the optical axis is

$$J_z = \frac{\lambda}{\alpha}\delta(0)\left[nI_0(2\alpha r_{0i}) + \frac{\alpha}{r_{0i}}\mathrm{Im}(y_0 x_0^*)I_1(2\alpha r_{0i})\right], \quad (16)$$

where $r_{0i} = [(\mathrm{Im}x_0)^2 + (\mathrm{Im}y_0)^2]^{1/2}, I_0(x), I_1(x)$ are modified Bessel functions, whereas the total power of the beam is

$$W = \frac{\delta(0)}{k\alpha}\int_0^{2\pi} \exp[2\alpha(\mathrm{Im}x_0\cos\theta + \mathrm{Im}y_0\sin\theta)]d\theta$$
$$= \frac{\lambda}{\alpha}\delta(0)I_0(2\alpha r_{0i}), \quad (17)$$

where $\delta(0)$ is the Dirac δ function at zero. From Eqs. (16) and (17), we can infer that although both the projection of OAM onto the optical axis and the power of the shifted Bessel beam are infinite, their ratio is finite:

$$\frac{J_z}{W} = n + \frac{\alpha}{r_{0i}}\mathrm{Im}(x_0^* y_0)\frac{I_1(2\alpha r_{0i})}{I_0(2\alpha r_{0i})}. \quad (18)$$

From Eq. (18) it follows that if the coordinates of the shift vector (x_0, y_0) are both purely real or purely imaginary, the normalized OAM in Eq. (18) equals that of a nonshifted Bessel beam:

$$\frac{J_z}{W} = n. \quad (19)$$

The normalized OAM of the shifted and nonshifted Bessel beams, Eqs. (18) and (19), will differ only when the shift is real on one coordinate and imaginary on the other. For instance, assuming $x_0 = b/\alpha$ and $y_0 = ic/\alpha$, the OAM in Eq. (18) takes the form:

$$\frac{J_z}{W} = n + b\frac{I_1(2|c|)}{I_0(2|c|)}. \quad (20)$$

It can be seen that at $b > 0$, the OAM in Eq. (20) is larger than that in Eq. (19), becoming smaller at $b < 0$. Note that the change of the beam shape is defined by the magnitude of the imaginary shift. The intensity pattern of the shifted beam in Eq. (13) takes the form of an ellipse at small $c < 1$ and is shaped as a semicrescent at $c > 1$, finally taking the form of an astigmatic Gaussian beam at $c >> 1$ [30]. On the x axis, the center of the Bessel beam in Eq. (5) is shifted by $\Delta x = (b - c)/\alpha$.

V. ORBITAL ANGULAR MOMENTUM OF THE SUPERPOSITION OF SHIFTED BESSEL BEAMS

Let us analyze the superposition of P shifted n-order Bessel beams of Eq. (13). Here the amplitude of angular spectrum of plane waves is given by

$$A(\rho,\theta) = \sum_{p=0}^{P-1} C_p A_{pn}(\rho,\theta), \quad (21)$$

where

$$A_{pn}(\rho,\theta) = \frac{(-i)^n}{\alpha\lambda}\exp(in\theta)\delta\left(\rho - \frac{\alpha}{\lambda}\right)$$
$$\times \exp[-ik\rho(x_p\cos\theta + y_p\sin\theta)] \quad (22)$$

is the amplitude of angular spectrum of the p-th constituent beam shifted by a complex vector with coordinates (x_p, y_p). Based on (14) and (15), the normalized OAM of the superposition in Eq. (21) is given by

$$\frac{J_z}{W} = n - i\alpha\frac{\sum_{p=0}^{P-1}\sum_{q=0}^{P-1} C_p^* C_q \frac{x_p^* y_q - x_q y_p^*}{R_{pq}} J_1(\alpha R_{pq})}{\sum_{p=0}^{P-1}\sum_{q=0}^{P-1} C_p^* C_q J_0(\alpha R_{pq})}, \quad (23)$$

where $J_0(x), J_1(x)$ are the Bessel functions of the zero and first order,

$$R_{pq} = \sqrt{(x_p^* - x_q)^2 + (y_p^* - y_q)^2},$$
$$R_{pp} = 2i\sqrt{(\mathrm{Im}x_p)^2 + (\mathrm{Im}y_p)^2}. \quad (24)$$

Although there is an imaginary factor $i\alpha$ in Eq. (23), the entire relation is real. This conclusion can be made from the facts that (i) at $p = q$, $|C_p|^2$ in the numerator is real, the magnitudes R_{pq} and $J_1(\alpha R_{pq})$ are purely imaginary, and the difference of two complex conjugated numbers $x_p^* y_p - x_p y_p^*$ is also purely imaginary and (ii) for any p and q, which are not equal to each other, $R_{pq} = R_{qp}^*$, whereas the terms with indices (p,q) and (q,p) also represent the difference of two complex conjugated numbers.

It can be shown that with all constituent Bessel beams in the superposition (21) shifted by a real vector (x_p, y_p) and all coefficients C_p assumed to be real, the numerator in (23) equals zero, so the total OAM of the superposition equals that of an individual nonshifted n-order Bessel beam in Eq. (19). This is a key finding of the present research. Based on it, it becomes possible to form the most diverse nonparaxial laser beams that would have different transverse intensity distributions but identical OAM of Eq. (19), while traveling without diffraction. Examples of such beams are discussed below.

From Eq. (23), interesting particular cases can be inferred. If $P = 2, x_0 = c/\alpha, y_0 = ic/\alpha, x_1 = c/\alpha, y_1 = ic/\alpha$, then $R_{00} = R_{11} = 2ic/\alpha, R_{01} = R_{10} = 0$, a simple expression for the normalized OAM can be derived [with the coefficients in Eq. (21) defined by arbitrary complex numbers C_0, C_1]:

$$\frac{J_z}{W} = n + \frac{c(|C_0|^2 - |C_1|^2)I_1(2|c|)}{(|C_0|^2 + |C_1|^2)I_0(2|c|) + 2\mathrm{Re}\{C_0^* C_1\}}. \quad (25)$$

Equation (25) suggests that in the superposition of two n-order Bessel beams with complex (purely imaginary) but matching shifts on one axis and equal coefficients $|C_0| = |C_1|$, the normalized OAM of Eq. (25) equals OAM of an individual nonshifted Bessel beam of n order, Eq. (19). Thus, assuming $|C_0| = |C_1|$, the transverse intensity pattern of the superposition of two shifted Bessel beams can be varied (because with varying c, the Bessel beam's shape varies), whereas the total OAM remains unchanged.

VI. SUPERPOSITION OF THREE SHIFTED BESSEL BEAMS

Below we analyze a superposition of three n-order Bessel beams that are shifted so their centers are found at the vertices of an equilateral triangle. Thus, in the superposition of Eq. (21), $P = 3, R_{01} = R_{02} = R_{12}$, the weight coefficients C_0, C_1, C_2 are arbitrary complex numbers, with the coordinates of the

complex shift vector assumed to be given by

$$\begin{cases} x_p = R_0 \cos\left(\frac{2\pi p}{3}\right) + \frac{c}{\alpha} \exp\left(-i\gamma - i\frac{2\pi p}{3}\right), \\ y_p = R_0 \sin\left(\frac{2\pi p}{3}\right) + i\frac{c}{\alpha} \exp\left(-i\gamma - i\frac{2\pi p}{3}\right), \end{cases} \tag{26}$$

where R_0 is the center of a circle on which the singularity centers of the shifted Bessel beams are found, c defines the asymmetry of the shifted Bessel beam, and γ is the angle of rotation of the asymmetric shifted Bessel beam. Then OAM is

$$\frac{J_z}{W} = n + \frac{\pm D_1 \xi I_1(2c) + \mathrm{Im}\{D_2(\xi \mp ic\sqrt{3}) J_1(\sqrt{3}\xi \pm ic)\}}{D_1 I_0(2c) + 2\mathrm{Re}\{D_2 J_0(\sqrt{3}\xi \pm ic)\}}, \tag{27}$$

with "+" taken for $\gamma = 0$ and "−" taken for $\gamma = \pi$,

$$\begin{aligned} D_1 &= |C_0|^2 + |C_1|^2 + |C_2|^2, \\ D_2 &= C_0^* C_1 + C_1^* C_2 + C_2^* C_0, \end{aligned} \tag{28}$$

where $\xi = \alpha R_0 \pm c$. In a particular case of $\gamma = \pi, c = \alpha R_0$, the ξ parameter equals zero and Eq. (27) is rearranged to

$$\frac{J_z}{W} = n + \frac{c\sqrt{3} I_1(c) \mathrm{Im}\{D_2\}}{D_1 I_0(2c) + 2 I_0(c) \mathrm{Re}\{D_2\}}. \tag{29}$$

From (29), we can infer that assuming real coefficients C_0, C_1, C_2, the term $\mathrm{Im}\{D_2\}$ in (29) equals zero and the OAM of the superposition of three shifted n-order Bessel beams equals OAM of an individual nonshifted Bessel beam of Eq. (19).

By way of illustration, Fig. 1 depicts the calculated (a) intensity pattern and (b) phase of the superposition of three shifted Bessel beams with topological charge $n = 3$. The OAM of the superposition is $J_z/W = 3$.

Figure 2 depicts the encoded phase [Fig. 2(a)] of the superposition of three shifted Bessel beams with topological charge $n = 3$ [Fig. 1(b)]. The phase was fed to a spatial light modulator SLM PLUTO-VIS (1920 × 1080 resolution, 8-μm pixel size).

Figures 2(b)–2(d) depicts the SLM-aided intensity patterns generated in reflection by the incident plane wave with linear polarization and wavelength of 633 nm at different distances. From Fig. 2, the beam is seen to preserve its structure upon propagation, and the intensity pattern is in agreement with the simulation results [Fig. 1(a)]. The intensity was measured with a complementary metal-oxide-semiconductor camera MDCE-5A (1/2 ″, 1280 × 1024 resolution).

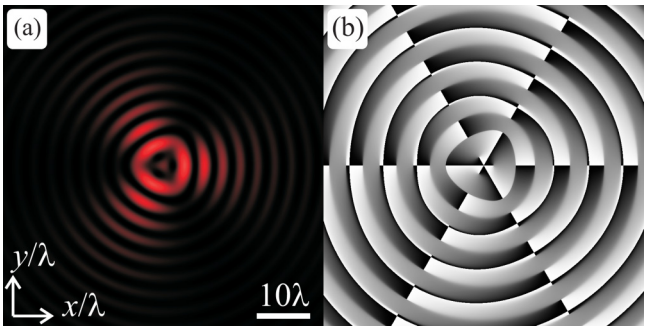

FIG. 1. (Color online) (a) Intensity and (b) phase (π, black; $-\pi$, white) of the superposition of three shifted Bessel beams with parameters: $n = 3$, $R_0 = 4\lambda$, $\alpha = 1/\lambda$, $c = 4$, $\gamma = \pi$, vector of weight coefficients $\mathbf{C} = [1,1,1]$. Frame size, $2R = 60\lambda$.

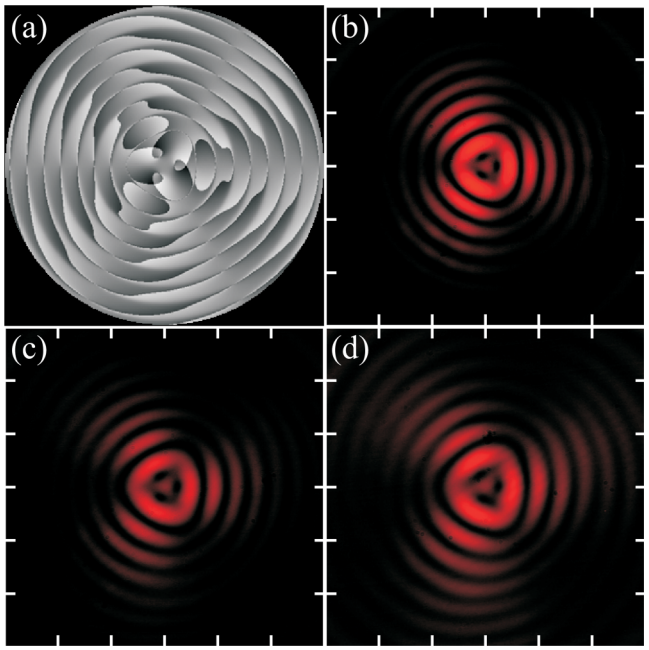

FIG. 2. (Color online) (a) Encoded phase [Fig. 1(b)] to generate a Bessel beam with the transverse intensity pattern shaped as an equilateral triangle and (b) experimentally generated intensity patterns at different distances from the plane $z = 0$: (b) 0 mm, (c) 200 mm, and (d) 400 mm. Mesh step (distance between the ticks) is 0.5 mm.

Figure 3 depicts the calculated phase and intensity distributions generated by the superposition of three shifted Bessel beams with identical weight coefficients, $\mathbf{C} = [1,1,1]$, taken at different values of the rest parameters: $n = 5$, $R_0 = 8\lambda$, and $c = 3$. In this case, the diffraction pattern differs entirely, with three bright spots being generated instead of an equilateral triangle. Because in this beam $c \neq \alpha R_0$, OAM cannot be derived from Eq. (29). According to Eq. (27), the OAM of this beam is fractional and equals

$$\frac{J_z}{W} = 5 + \frac{\mathrm{Im}\{(5 + i3\sqrt{3}) J_1(5\sqrt{3} - 3i)\} - 5 I_1(6)}{I_0(6) + 2\mathrm{Re}\{J_0(5\sqrt{3} - 3i)\}} \approx 0.62.$$

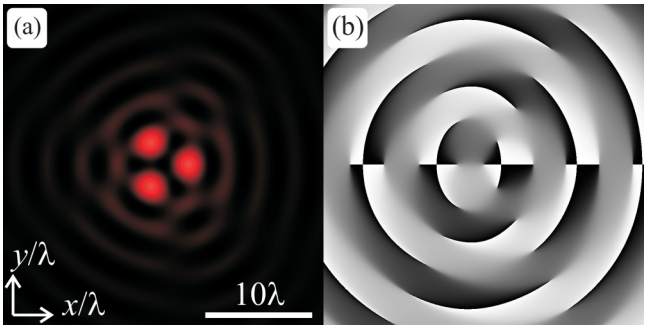

FIG. 3. (Color online) Calculated (a) intensity and (b) phase (π, black; $-\pi$, white) patterns generated by the superposition of three shifted Bessel beams with parameters $n = 5$, $R_0 = 8\lambda$, $\alpha = 1/\lambda$, $c = 3$, $\gamma = \pi$, weight coefficient vector, $\mathbf{C} = [1,1,1]$. Frame size, $2R = 30\lambda$.

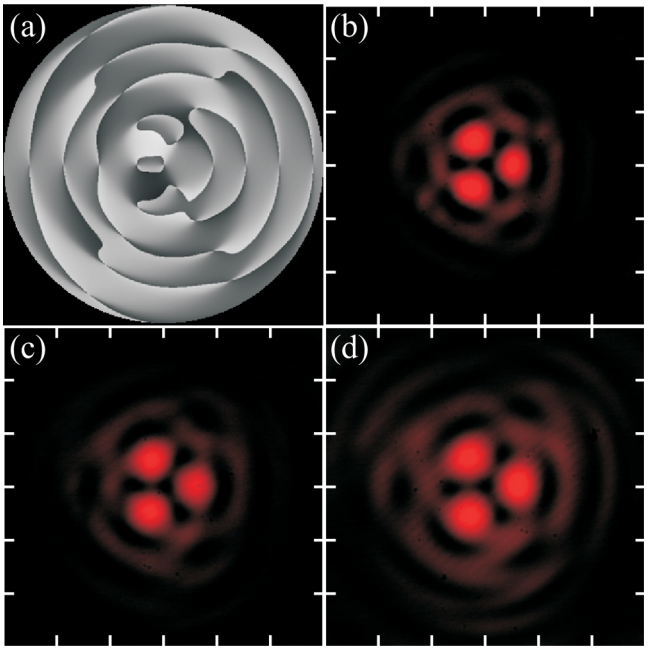

FIG. 4. (Color online) (a) Encoded phase to generate the superposition of three Bessel beams with the transverse intensity pattern featuring three bright spots [Fig. 3(a)] and experimentally generated intensity patterns at different distances from the plane $z = 0$: (b) 0 mm, (c) 200 mm, and (d) 400 mm. Mesh step (distance between the ticks), 0.5 mm.

Figure 4 depicts the SLM-aided [Fig. 4(a)] phase and [Figs. 4(b)–4(d)] intensity patterns generated at different distances by the superposition of three shifted Bessel beams with parameters $n = 5$, $R_0 = 8\lambda$, $\alpha = 1/\lambda$, $c = 3$, and $\gamma = \pi$. From Fig. 4, the experimental diffraction patterns are seen to be in agreement with the calculated intensity distribution in Fig. 3(a).

VII. SUPERPOSITION OF IDENTICAL BESSEL BEAMS FOUND AT THE VERTICES OF A REGULAR POLYGON

As in the previous case, we shall analyze the superposition of P shifted n-order Bessel beams with their singularity centers found at the vertices of a regular polygon [similar to (26)]:

$$\begin{aligned} x_p &= R_0 \cos\left(\frac{2\pi p}{P}\right) + \frac{c}{\alpha}\exp\left(-i\gamma - i\frac{2\pi p}{P}\right), \\ y_p &= R_0 \sin\left(\frac{2\pi p}{P}\right) + i\frac{c}{\alpha}\exp\left(-i\gamma - i\frac{2\pi p}{P}\right). \end{aligned} \tag{30}$$

where $p = 0, \ldots, P-1$.

For certainty, assume $\gamma = \pi$ and $c = \alpha R_0$. Then we have, instead of (30),

$$\begin{aligned} x_p &= iR_0 \sin\left(\frac{2\pi p}{P}\right), \\ y_p &= -iR_0 \cos\left(\frac{2\pi p}{P}\right). \end{aligned} \tag{31}$$

The general relationship for the OAM of Eq. (23) takes the form:

$$\frac{J_z}{W} = n + \alpha\frac{2R_0\sum_{p=1}^{P-1}\sum_{q=0}^{p-1}\mathrm{Im}\{C_p^* C_q\}\sin\left[\frac{\pi(p-q)}{P}\right] I_1\left\{2\alpha R_0\left[\frac{\pi(p-q)}{P}\right]\right\}}{\sum_{p=0}^{P-1}|C_p|^2 I_0(2\alpha r_{pi}) + 2\sum_{p=1}^{P-1}\sum_{q=0}^{p-1}\mathrm{Re}\{C_p^* C_q J_0(\alpha R_{pq})\}}. \tag{32}$$

With all coefficients C_p assumed to be real, the numerator in Eq. (32) equals zero and OAM of the superposition of shifted Bessel beams equals that of an individual nonshifted Bessel beam in Eq. (19). By way of illustration, Fig. 5 depicts the numerically simulated intensity pattern and phase for the superposition of four shifted Bessel beams with topological charge $n = 7$. The normalized OAM of the superposition equals $J_z/W = 7$. As seen in Fig. 5(b), within a main squarelike intensity ring there are seven optical vortices with topological charge $+1$.

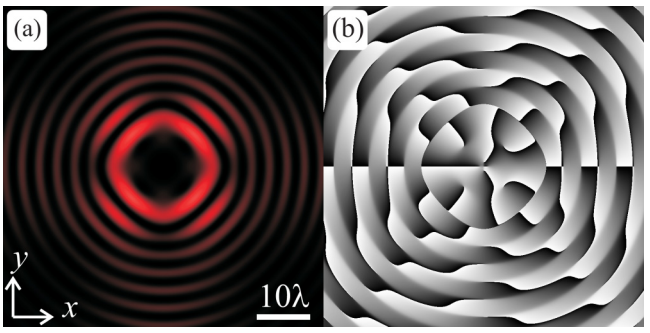

FIG. 5. (Color online) (a) Intensity and (b) phase (π, black; $-\pi$, white color) of a superposition of four ($P = 4$) shifted Bessel beam with parameters $n = 7$, $R_0 = 6\lambda$, $\alpha = 1/\lambda$, $c = 6$, $\gamma = \pi$, $\mathbf{C} = [1,1,1,1]$. Frame size, $2R = 60\lambda$.

Figure 6 depicts the SLM-aided encoded phase [Fig. 6(a)] and intensity patterns [Figs. 6(b)–6(d)] generated at different distances by the superposition of four shifted Bessel beams (Fig. 5) with topological charge $n = 7$, $R_0 = 6\lambda$, $\alpha = 1/\lambda$, $c = 6, \gamma = \pi, \mathbf{C} = [1,1,1,1]$. The diffraction patterns in Fig. 6 are seen to be in good agreement with the simulated intensity patterns in Fig. 5(a).

Another example in Fig. 7 shows [Fig. 7(a)] the intensity and [Fig. 7(b)] phase of the superposition of six ($P = 6$) shifted Bessel beams with the same topological charge $n = 10$, with their singularity centers found at the vertices of a regular hexagon. The normalized OAM of the superposition equals $J_z/W = 10$.

Figure 8 depicts [Fig. 8(a)] SLM-aided encoded phase and [Figs. 8(b)–8(d)] intensity pattern generated at different distances by the superposition of six ($P = 6$) shifted Bessel beams (Fig. 7) with the same topological charge $n = 10$ at

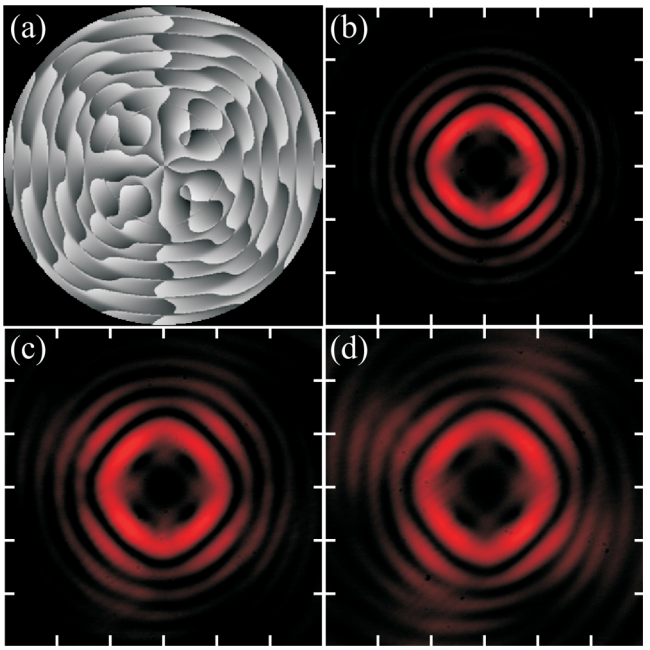

FIG. 6. (Color online) SLM-aided (a) encoded phase of Fig. 5(b) to generate the superposition of four shifted Bessel beams with a square-shaped transverse intensity distribution and experimental intensity patterns at different distances from the plane $z = 0$: (b) 0 mm, (c) 200 mm, and (d) 400 mm. Mesh step (distance between the ticks), 0.5 mm.

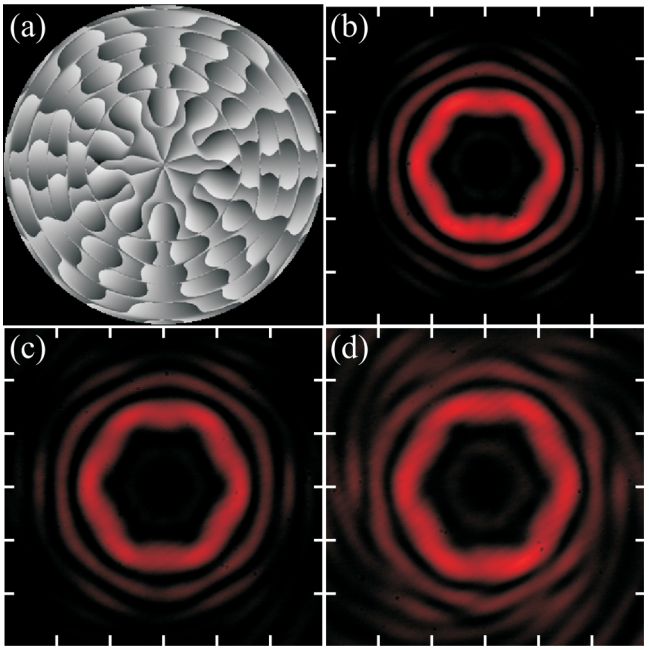

FIG. 8. (Color online) (a) SLM-aided encoded phase [Fig. 7(a)] to generate the superposition of six shifted Bessel beams with a hexagon-shaped transverse intensity distribution and experimental intensity patterns at different distances from the plane $z = 0$: (b) 0 mm, (c) 200 mm, and (d) 400 mm. Mesh step (distance between the ticks), 0.5 mm.

$R_0 = 12\lambda$, $\alpha = 1/\lambda$, $c = 12$, $\gamma = \pi$, $\mathbf{C} = [1,1,1,1,1,1]$. The diffraction patterns in Fig. 8 are seen to be in good agreement with the simulation results in Fig. 7(a).

VIII. SUPERPOSITION OF A LARGE NUMBER OF BESSEL BEAMS CENTERED ON A CIRCLE

In this section, we show that putting the center of a shifted n-order Bessel beam at each point of a circle of radius R_0 and taking the superposition of an infinite number of such beams with identical weight coefficients, their superposition will generate a conventional nonshifted n-order Bessel beam.

Describing the Bessel function as a series, the nonshifted Bessel beam in Eq. (5) can also be presented as a series in the plane $z = 0$:

$$E(x,y,z=0) = \exp(in\phi)J_n(\alpha r) = \sum_{p=0}^{\infty} \frac{(-1)^p}{p!(n+p)!} \times \left(\frac{\alpha}{2}\right)^{n+2p} (x-iy)^p (x+iy)^{n+p}. \quad (33)$$

The continuous superposition of the shifted Bessel beams of Eq. (33) centered on a circle of radius R_0 is given by

$$E(x,y,z=0) = \sum_{p=0}^{\infty} \frac{(-1)^p}{p!(n+p)!} \left(\frac{\alpha}{2}\right)^{n+2p} \times \int_0^{2\pi} [(x - R_0\cos\theta) - i(y - R_0\sin\theta)]^p \times [(x - R_0\cos\theta) + i(y - R_0\sin\theta)]^{n+p} d\theta. \quad (34)$$

In polar coordinates, Eq. (34) takes the form:

$$E(r,\phi,z=0) = \sum_{p=0}^{\infty} \frac{(-1)^p}{p!(n+p)!} \left(\frac{\alpha}{2}\right)^{n+2p} \times \int_0^{2\pi} [r\exp(-i\phi) - R_0\exp(-i\theta)]^p \times [r\exp(i\phi) - R_0\exp(i\theta)]^{n+p} d\theta. \quad (35)$$

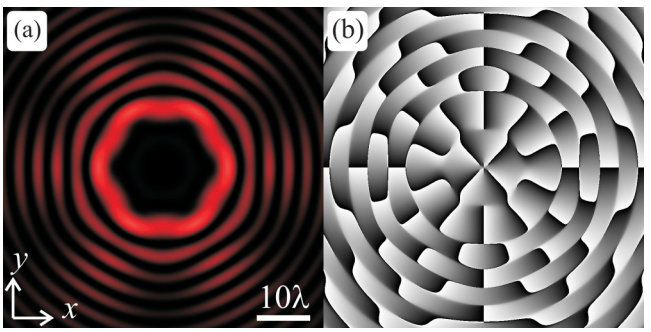

FIG. 7. (Color online) Simulated (a) intensity and (b) phase (π, black; -π, white) of the superposition of six shifted Bessel beams with parameters $P = 6, n = 10, R_0 = 12\lambda, \alpha = 1/\lambda, c = 12, \gamma = \pi$, $\mathbf{C} = [1,1,1,1,1,1]$. Frame size, $2R = 60\lambda$.

Both integrand terms in Eq. (35) can be given as a binomial expansion:

$$E(r,\phi,z=0) = \sum_{p=0}^{\infty} \frac{(-1)^p}{p!(n+p)!}\left(\frac{\alpha}{2}\right)^{n+2p} \times \sum_{s=0}^{p}\sum_{t=0}^{n+p}\binom{p}{s}\binom{n+p}{t}(-R_0)^{s+t} r^{2p-s+n-t} \times \exp[i(n+p-t)\phi - i(p-s)\phi] \times \int_0^{2\pi} \exp[i(t-s)\theta]d\theta. \quad (36)$$

Considering that integral (36) over θ takes a nonzero value only at $t = s$, the sum over t drops out and Eq. (36) is reduced to

$$E(r,\phi,z=0) = 2\pi \exp(in\phi) \sum_{p=0}^{\infty} \frac{(-1)^p}{p!(n+p)!}\left(\frac{\alpha r}{2}\right)^{n+2p} \times \sum_{s=0}^{p}\binom{p}{s}\binom{n+p}{s}\left(\frac{R_0}{r}\right)^{2s}. \quad (37)$$

Changing the order of summation in Eq. (37), we obtain:

$$\begin{aligned} E(r,\phi,z=0) &= 2\pi \exp(in\phi)\left[\sum_{s=0}^{\infty}\left(\frac{R_0}{r}\right)^{2s} \times \sum_{p=s}^{\infty}\binom{p}{s}\binom{n+p}{s}\frac{(-1)^p}{p!(n+p)!}\left(\frac{\alpha r}{2}\right)^{n+2p}\right] \\ &= 2\pi \exp(in\phi)\sum_{s=0}^{\infty}\left(\frac{R_0}{r}\right)^{2s} \times \sum_{p=s}^{\infty}\frac{(-1)^p}{(s!)^2(p-s)!(n+p-s)!}\left(\frac{\alpha r}{2}\right)^{n+2p}. \end{aligned} \quad (38)$$

Replacing $p - s$ with p and regrouping the terms of both series, we can reduce the above relation to Bessel functions:

$$\begin{aligned} E(r,\phi,z=0) &= 2\pi \exp(in\phi)\left[\sum_{s=0}^{\infty}\frac{(R_0/r)^{2s}}{(s!)^2} \times \sum_{p=0}^{\infty}\frac{(-1)^{p+s}}{p!(n+p)!}\left(\frac{\alpha r}{2}\right)^{n+2p+2s}\right] \\ &= 2\pi \exp(in\phi)\left[\sum_{s=0}^{\infty}\frac{(-1)^s}{(s!)^2}\left(\frac{\alpha R_0}{2}\right)^{2s}\right] \times \left[\sum_{p=0}^{\infty}\frac{(-1)^p}{p!(n+p)!}\left(\frac{\alpha r}{2}\right)^{n+2p}\right] \\ &= 2\pi J_0(\alpha R_0) J_n(\alpha r)\exp(in\phi). \end{aligned} \quad (39)$$

Equation (39) describes the amplitude of a conventional Bessel beam up to a constant term $2\pi J_0(\alpha R_0)$. Figure 9 depicts simulated superpositions of 5, 8, 10, 20, 40, and 60 shifted Bessel beams with topological charge $n = 7$, centered on a circle of radius $R_0 = 100\lambda$. For all beams shown in Figs. 9(a)–9(f), simulation parameters were the same: $n = 7$, $R_0 = 100\lambda$, $\alpha = 1/\lambda$. Frame size was $2R = 240\lambda$.

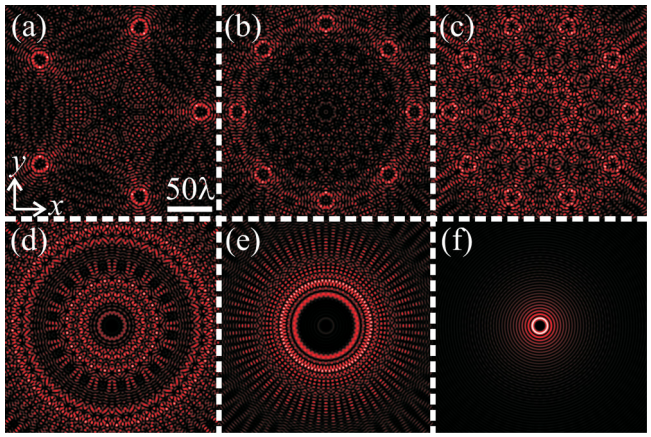

FIG. 9. (Color online) Transverse intensity distribution of the superposition of P shifted Bessel beams at $P = 5$ (a), 8 (b), 10 (c), 20 (d), 40 (e), and 60 (f). Frame size in all figures is $240\lambda \times 240\lambda$.

From Fig. 9, a near-nonshifted or conventional Bessel mode is seen to be generated already at $P = 60$, with its amplitude defined by Eq. (39). All superpositions in Figs. 9(a)–9(f) have the same normalized OAM, which is equal to $J_z/W = 7$.

Figure 10 depicts [Fig. 10(a)] SLM-aided encoded phase (1024×1024 pixels) and [Figs. 9(b)–10(d)] intensity patterns generated at different distances by the superposition of 40 ($P = 40$) shifted Bessel beams [Fig. 9(e)] with topological charge $n = 7$, centered on a circle of radius $R_0 = 3.33$ mm.

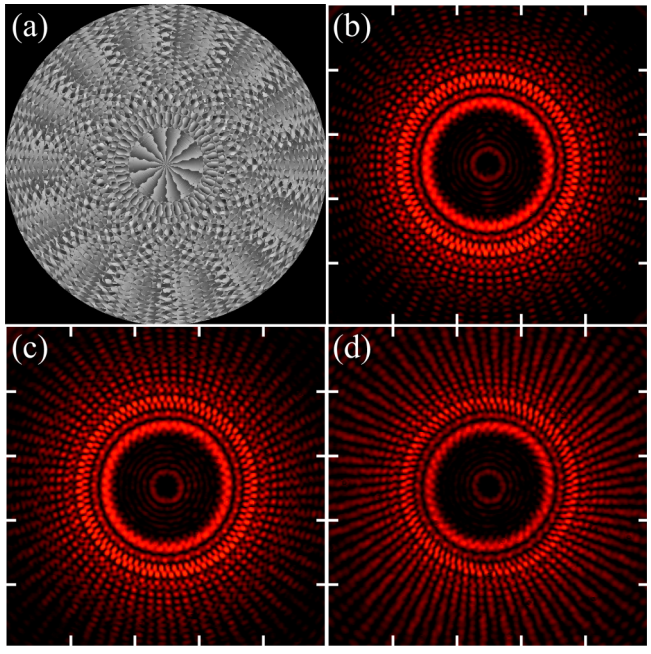

FIG. 10. (Color online) (a) SLM-aided encoded phase to generate the superposition of 40 shifted Bessel beams and experimental intensity patterns at different distances from the plane $z = 0$: (b) 0 mm, (c) 50 mm, and (d) 100 mm. Mesh step (distance between the ticks), 0.5 mm.

The SLM-encoded element has the size of 8×8 mm, scaling factor α of the Bessel beams equals to 30 mm^{-1}. Such values of parameters are chosen to match the numerically obtained Fig. 9(e): The picture size $2R = 240\lambda$ in Fig. 9(e) matches $2R = 8$ mm in Fig. 10(a), the scaling factor $\alpha = 1/\lambda$ in Fig. 9(e) matches $\alpha = 30\,\text{mm}^{-1}$ in Fig. 10(a), and the radius of the circle $R_0 = 100\lambda$ in Fig. 9(e) matches $R_0 = 3.33$ mm in Fig. 10(a). The diffraction patterns in Fig. 10 are seen to be in good agreement with the simulation results in Fig. 9(e).

In all considered cases the α parameter of the Bessel beam (5) was chosen as $\alpha = k \sin\theta = 1/\lambda$, where θ is half of inclination angle of the conical wave generating the Bessel beam. In [35] the paraxiality parameter has been introduced for the Gaussian-like beams: $f = w/l = 1/(kw) = \tan\theta$, where w is the Gaussian beam waist radius, l is the Rayleigh range, and θ is half of the beam's divergence angle. The similar parameter for the Bessel beam equals $f' = \alpha/k = \sin\theta$. In our case $f' = 1/(2\pi)$. The nondiffracting range for the Bessel beam is $l_{\text{ND}} = R/\tan\theta \approx Rk/\alpha$ [1]. So, for example, the beam in Fig. 1 has the range $l_{ND} = 30\lambda(2\pi/\lambda)/(1/\lambda) = 60\pi\lambda$.

IX. CONCLUSION

To summarize, the normalized OAM of the superposition of shifted Bessel beams with identical topological charge has been derived in an analytical form, Eq. (23). It has been shown that if all weight coefficients of the constituent terms in the superposition of shifted Bessel beams are real, the total OAM of the superposition equals that of an individual nonshifted Bessel beam. Based on this property, nondiffractive beams that have different intensity distributions but the same OAM can be generated (Fig. 9). The superposition of a large number of identical Bessel beams centered on an arbitrary-radius circle has been shown to be equivalent to an individual constituent Bessel beam found at the circle center [Eq. (39)]. It has been also shown that a complex shift of a Bessel beam causes changes in the transverse intensity distribution, also changing OAM [Eqs. (18) and (20)]. In the superposition of two complex-shifted Bessel beams, the OAM may remain unchanged, meanwhile the intensity distribution will change, Eq. (25).

The experiment has been shown to be in good agreement with theory (Figs. 2, 4, 6, 8, and 10).

ACKNOWLEDGMENTS

The work was partially funded by the Russian Federation Ministry of Education and Science, Russian Federation Presidential grants for support of leading scientific schools (Grant No. NSh-3970.2014.9) and Russian Foundation of Basic Research Grants No. 13-07-97008, No. 14-29-07133, No. 14-07-31092, No. 15-07-01174, and No. 15-37-20723.

[1] J. Durnin, J. Opt. Soc. Am. A **4**, 651 (1987).
[2] J. Durnin, J. J. Miceli, and J. H. Eberly, Phys. Rev. Lett. **58**, 1499 (1987).
[3] J. Turunen, A. Vasara, and A. T. Friberg, Appl. Opt. **27**, 3959 (1988).
[4] A. Vasara, J. Turunen, and A. T. Friberg, J. Opt. Soc. Am. A **6**, 1748 (1989).
[5] R. P. MacDonald, S. A. Boothroyd, T. Okamato, J. Chrostowski, and B. A. Syrett, Opt. Commun. **122**, 169 (1996).
[6] C. A. McQueen, J. Arlt, and K. Dholakia, Am. J. Phys. **67**, 912 (1999).
[7] S. M. Barnett and L. Allen, Opt. Commun. **110**, 670 (1994).
[8] K. Volke-Sepulveda, V. Garces-Chavez, S. Chavez-Cedra, J. Arlt, and K. Dholakia, J. Opt. B: Quant. Semiclass. Opt. **4**, S82 (2002).
[9] V. V. Kotlyar, S. N. Khonina, and V. A. Soifer, J. Mod. Opt. **42**, 1231 (1995).
[10] V. V. Kotlyar, S. N. Khonina, and V. A. Soifer, J. Mod. Opt. **44**, 1409 (1997).
[11] P. Paakkonen, J. Lautanen, M. Honkanen, M. Kuittinen, J. Turunen, S. N. Khonina, V. V. Kotlyar, V. A. Soifer, and A. T. Friberg, J. Mod. Opt. **45**, 2355 (1998).
[12] S. N. Khonina, V. V. Kotlyar, V. A. Soifer, J. Lautanen, M. Honkanen, and J. Turunen, Optik **112**, 137 (1999).
[13] H. S. Lee, B. W. Stewart, K. Choi, and H. Fenichel, Phys. Rev. A **49**, 4922 (1994).
[14] R. M. Herman and T. A. Wiggins, J. Opt. Soc. Am. A **8**, 932 (1991).
[15] J. Arlt and K. Dholakia, Opt. Commun. **177**, 297 (2000).
[16] V. V. Kotlyar, S. N. Khonina, V. A. Soifer, G. V. Uspleniev, and M. V. Shinkarev, Opt. Commun. **91**, 158 (1992).
[17] J. A. Devis, E. Carcole, and D. M. Cottrell, Appl. Opt. **35**, 593 (1996).
[18] S. N. Khonina, V. V. Kotlyar, V. A. Soifer, K. Jefimovs, P. Paakkonen, and J. Turunen, J. Mod. Opt. **51**, 677 (2004).
[19] M. P. MacDonald, L. Paterson, K. Volke-Sepulveda, J. Arlt, W. Sibbett, and K. Dholakia, Science **296**, 1101 (2002).
[20] V. Garces-Chavez, D. McGloin, H. Melville, W. Sibbett, and K. Dholakia, Nature **419**, 145 (2002).
[21] S. N. Khonina, V. V. Kotlyar, R. V. Skidanov, V. A. Soifer, K. Jefimovs, J. Simonen, and J. Turunen, J. Mod. Opt. **51**, 2167 (2004).
[22] J. Arlt, T. Hitomi, and K. Dholakia, Appl. Phys. B **71**, 549 (2000).
[23] J. Arlt, K. Dholakia, J. Soneson, and E. M. Wright, Phys. Rev. A **63**, 063602 (2001).
[24] V. V. Kotlyar, A. A. Kovalev, and V. A. Soifer, J. Opt. Soc. Am. A **29**, 741 (2012).
[25] Y. Zhu, X. Liu, J. Gao, Y. Zhang, and F. Zhao, Opt. Express **22**, 7765 (2014).
[26] Z. Bouchal and M. Olivik, J. Mod. Opt. **42**, 1555 (1995).
[27] Y.-Z. Yu and W.-B. Dou, Progress In Electromagnetics Research Letters **5**, 57 (2008).
[28] I. A. Litvin, A. Dudley, and A. Forbes, Opt. Express **19**, 16760 (2011).
[29] Y. F. Chen, Y. C. Lin, W. Z. Zhuang, H. C. Liang, K. W. Su, and K. F. Huang, Phys. Rev. A **85**, 043833 (2012).

[30] V. V. Kotlyar, A. A. Kovalev, and V. A. Soifer, Opt. Lett. **39**, 2395 (2014).
[31] V. V. Kotlyar, A. A. Kovalev, R. V. Skidanov, and V. A. Soifer, J. Opt. Soc. Am. A **31**, 1977 (2014).
[32] L. Gong, X. Qui, Y. Ren, H. Zhu, W. Liu, and J. Zhou, Opt. Express **22**, 26763 (2014).
[33] C. J. R. Sheppard, S. S. Kou, and J. Lin, J. Opt. Soc. Am. A **31**, 2674 (2014).
[34] J. W. Goodman, *Introduction to Fourier Optics* (McGraw-Hill, New York, 1968).
[35] M. Lax, W. Louisell, and W. B. McKnight, Phys. Rev. A **11**, 1365 (1975).